J|A|C|S
ARTICLES
Published on Web 05/02/2006

Nucleophilic−Alkylation−Reoxidation: A Functionalization Sequence for Single-Wall Carbon Nanotubes

Ralf Graupner,*,† Jürgen Abraham,‡ David Wunderlich,‡ Andrea Vencelová,† Peter Lauffer,† Jonas Röhrl,† Martin Hundhausen,† Lothar Ley,† and Andreas Hirsch*,‡

Contribution from the Technische Physik, Universität Erlangen, Erwin-Rommel-Strasse 1, 91058 Erlangen, Germany, and Institut für Organische Chemie II, Universität Erlangen, Henkestrasse 42, 91054 Erlangen, Germany

Received January 31, 2006; E-mail: ralf.graupner@physik.uni-erlangen.de; andreas.hirsch@chemie.uni-erlangen.de

Abstract: A new reaction sequence for the chemical functionalization of single-wall carbon nanotubes (SWNTs) consisting of the nucleophilic addition of *t*-BuLi to the sidewalls of the tubes and the subsequent reoxidation of the intermediates *t*-Bu$_n$SWNT^{n-} leading to *t*-Bu$_n$SWNT was developed. During the formation of the *t*-Bu$_n$SWNT^{n-}, a homogeneous dispersion in benzene was formed due to the electrostatic repulsion of the negatively charged intermediates causing debundling. The entire reaction sequence can be repeated, and the degree of functionalization of the products (*t*-Bu$_n$)$_m$SWNT ($m = 1-3$) increases with increasing *m*. Degrees of functionalization expressed as the carbon-to-addend ratio of up to 31 were reached. The reaction was studied in detail by photoelectron spectroscopy, Raman spectroscopy, and scanning tunneling microscopy (STM). The C 1s core level spectra reveal that the nucleophilic attack of the *t*-BuLi leads to negatively charged SWNTs. Upon oxidation, this negative charge is removed. The valence band spectra of the functionalized samples exhibit a significant reduction in the π-derived density of states. In STM, the covalently bonded *t*-butyl groups attached to the sidewalls have been visualized. Raman spectroscopy reveals that addition of the nucleophile to metallic tubes is preferred over the addition to semiconducting tubes.

Introduction

In the past few years, the chemical sidewall functionalization of carbon nanotubes, especially of single-wall carbon nanotubes (SWNTs), has become a challenging field of research.[1−8] The modification of the properties of the tubes is considered to be very promising. Moreover, this new nanochemistry allows for the combination of the unprecedented material properties of the tubes with those of other types of materials. In contrast to the chemical modification of small and well-defined organic molecules including the fullerenes,[9] the functionalization of SWNTs is associated with many additional problems.[1] The most important ones are (a) insolubility, (b) aggregation into bundles of different diameters, (c) wide variation of the helicities, (d) presence of defects, both at the tube ends and on the sidewalls, and (e) great variation of the tubes lengths. As compared to the fullerenes, another complication is the less pronounced pyramidalization of the C-atoms of the sidewalls. As a consequence, the ease of covalent attachment of addends, which is driven by reduction of strain energy stored in the pyramidalized C-atoms, is much lower than that of, for example, C_{60}.[10] Only comparatively harsh reaction conditions or "hot" addends such as fluorine,[11] radicals,[12,13] carbenes,[12,14] nitrenes,[12] azomethine ylides,[15] butyllithium,[16−18] and diazonium salts[19,20] are suitable for successful sidewall attacks to SWNTs. Control over regio- and chemoselectivity is very hard to achieve. An important prerequisite for a comparatively even functionalization of the tubes (individually functionalized carbon nanotubes) is the

† Technische Physik.
‡ Institut für Organische Chemie II.

(1) Hirsch, A. *Angew. Chem., Int. Ed.* **2002**, *41*, 1853−1859.
(2) Hirsch, A.; Vostrowsky, O. *Top. Curr. Chem.* **2005**, *245*, 193−237.
(3) Vostrowsky, O.; Hirsch, A. *Angew. Chem., Int. Ed.* **2004**, *43*, 2326−2329.
(4) Bahr, J. L.; Tour, J. M. *J. Mater. Chem.* **2002**, *12*, 1952−1958.
(5) Haddon, R. C. *Acc. Chem. Res.* **2002**, *35*, 997.
(6) Niyogi, S.; Hamon, M. A.; Hu, H.; Zhao, B.; Bhowmik, P.; Sen, R.; Itkis, M. E.; Haddon, R. C. *Acc. Chem. Res.* **2002**, *35*, 1105−1113.
(7) Sun, Y.-P.; Fu, K.; Lin, Y.; Huang, W. *Acc. Chem. Res.* **2002**, *35*, 1096−1104.
(8) Banerjee, S.; Hemraj-Benny, T.; Wong, S. S. *Adv. Mater.* **2005**, *17*, 17−29.
(9) Hirsch, A.; Brettreich, M.; *Fullerenes: Chemistry and Reaction*; Wiley-VCH: Weinheim, 2005.
(10) Chen, Z.; Thiel, W.; Hirsch, A. *ChemPhysChem* **2003**, *4*, 93−97.
(11) Mickelson, E. T.; Huffman, C. B.; Rinzler, A. G.; Smalley, R. E.; Hauge, R. H.; Margrave, J. L. *Chem. Phys. Lett.* **1998**, *296*, 188−194.
(12) Holzinger, M.; Vostrowsky, O.; Hirsch, A.; Hennrich, F.; Kappes, M.; Weiss, R.; Jellen, F. *Angew. Chem., Int. Ed.* **2001**, *40*, 4002−4005.
(13) Peng, H.; Reverdy, P.; Khabashesku, V. N.; Margrave, J. L. *Chem. Commun.* **2003**, 362−363.
(14) Chen, H. S.; Kortan, A. R.; Haddon, R. C.; Kopylov, N. *J. Phys. Chem.* **1993**, *97*, 3088−3090.
(15) Georgakilas, V.; Kordatos, K.; Prato, M.; Guldi, D. M.; Holzinger, M.; Hirsch, A. *J. Am. Chem. Soc.* **2002**, *124*, 760−761.
(16) Viswanathan, G.; Chakrapani, N.; Yang, H.; Wei, B.; Chung, H.; Cho, K.; Ryu, C. Y.; Ajayan, P. M. *J. Am. Chem. Soc.* **2003**, *125*, 9258−9259.
(17) Blake, R.; Gun'ko, Y. K.; Coleman, J.; Cadek, M.; Fonseca, A.; Nagy, J. B.; Blau, W. J. *J. Am. Chem. Soc.* **2004**, *126*, 10226−10227.
(18) Chen, S.; Shen, W.; Wu, G.; Chen, D.; Jiang, M. *Chem. Phys. Lett.* **2005**, *402*, 312−317.
(19) Bahr, J. L.; Yang, J.; Kosynkin, D. V.; Bronikowski, M. J.; Smalley, R. E.; Tour, J. M. *J. Am. Chem. Soc.* **2001**, *123*, 6536−6542.
(20) Bahr, J. L.; Tour, J. M. *Chem. Mater.* **2001**, *13*, 3823−3824.

10.1021/ja0607281 CCC: $33.50

exfoliation and dissolution of the bundles either before or during the attachment of the addends. Two elegant examples for such functionalization reactions involving the complete debundling of tubes were reported by Tour and co-workers[21] as well as by Billups and co-workers.[22,23] In the first case, the exfoliation of the tubes was achieved by wrapping the tubes in dodecyl sulfate (SDS) prior to the reaction with diazonium salts. The second method relies on the electrostatic repulsion of negatively charged SWNTs[24] obtained from Birch reduction before electrophilic addition of alkylhalides is allowed to take place. Whereas it is one challenge to find suitable conditions for satisfactory nanotube functionalization, the characterization of the reaction products is another. Only a combination of several analytical methods can be used to demonstrate unambiguously that functionalization has taken place.[25] Moreover, many of the traditional characterization tools of organic chemistry, like conventional mass spectroscopy and NMR, cannot be used for the investigation of functionalized SWNTs. Instead, electronic absorption spectroscopy and Raman spectroscopy provide direct insight into the modification of the electronic structures of the tubes. In combination with TGA- and XPS-investigations, an estimation of the degree of functionalization can be obtained. Microscopic methods such as TEM or AFM are very useful for the characterization because they can be applied to decide whether individualization of the bundles has occurred. NMR or IR spectroscopy as the sole characterization methods are unsuitable because based on the quality of functionalized tubes currently at hand they cannot distinguish between covalently functionalized tubes and mechanical mixtures of the components. The current state-of-the-art of the characterization of functionalized SWNTs is best described in a review by Tour et al.[25]

In this work, we report for the first time a new reaction sequence for the functionalization of SWNTs, their treatment with *t*-butyllithium (*t*-BuLi) and the subsequent reoxidation of the negatively charged intermediates with air oxygen to give the neutral derivatives *t*-Bu$_n$SWNT. At the beginning of the development of fullerene chemistry, we studied related reactions to functionalize C_{60} and discovered that protonation of the intermediate fullerene anions such as RC_{60}^- affords regioselectively the organo-1,2-dihydrofullerenes HRC_{60}.[26,27] On the other hand, it was found that the negatively charged intermediates can easily be oxidized by air oxygen to give neutral adducts such as R_2C_{60}.[9] The treatment of nanotubes with organolithium compounds leading to the formation of the proposed negatively charged intermediates R$_n$SWNT^{n-} has literature precedence[16−18] and was used to initiate polymerization or to couple functional polymers. The description of the resulting polymer functionalized SWNTs was the main focus of these contributions, and the subsequent reoxidation has not been considered to terminate the functionalization process. Next to the development of the nucleophilic−alkylation−reoxidation−functionalization of SWNTs, we present here a careful and systematic investigation of the entire functionalization sequence. Photoelectron spectroscopy allows us to investigate charging effects in SWNTs, which show up as shifts in binding energy of all spectral features.[28,29] Additionally, changes in the π-bonded electron system of SWNTs show up in the characteristic loss features of the C 1s core level as well as in the valence band spectra of the SWNTs. Raman spectroscopy and TGA were used (a) to independently verify the successful derivatization, (b) to estimate the degree of functionalization, and (c) to prove that unfunctionalized tubes can be recovered after thermal cleavage of the addends. Moreover, as Raman spectroscopy is selective to a subset of an ensemble of SWNTs due to the resonant nature of the scattering process,[30−33] an investigation of the radial breathing modes (RBMs) allows us to show that metallic tubes are more reactive toward the addition of carbon nucleophiles than are semiconducting tubes. Finally, to get a more detailed picture of the changes at the surface of individual SWNTs, we performed scanning tunneling microscopy (STM) and present the direct visualization of covalently bound addends at the sidewall of the tubes.

Results and Discussion

Synthesis. As starting material for the sidewall functionalization, we used the commercially available purified HiPco SWNTs (Carbon Nanotechnologies Inc., Houston, TX). Prior to the reaction with *t*-BuLi in an inert gas atmosphere, the tubes were dispersed in anhydrous benzene in an ultrasonic bath to ensure a wetting of the SWNTs by the solvent (Scheme 1). The resulting suspension is unstable, because the removal from the ultrasonic bath leads to the reagglomeration of the SWNTs. An excess of a solution of the *t*-BuLi was added slowly to this suspension, and the mixture was stirred for 30 min and ultrasonicated for another 30 min at room temperature to facilitate a uniform access of the *t*-BuLi to the SWNTs. We note that in previous experiments we were not able to detect a noticeable amount of defects introduced by our sonication technique alone. During the addition of the *t*-BuLi, a black and very homogeneous dispersion of the tubes was formed and no particles could be seen anymore. This observation is consistent with the proposed nucleophilic attack of the very nucleophilic *t*-BuLi compounds to the sidewalls of the tubes accompanied by a transfer of negative charge to the SWNTs. The subsequent homogeneous dispersion of the reaction intermediates *t*-Bu$_n$-SWNT^{n-} in benzene is a result of the repulsive interaction between the negatively charged nanotubes leading to a considerable exfoliation of the bundles (Scheme 1). Such dispersions were stable for approximately 1 day under the applied inert conditions.

The reaction intermediates *t*-Bu$_n$SWNT^{n-} were subsequently reoxidized by bubbling oxygen through the homogeneous

(21) Dyke, C. A.; Tour, J. M. *Nano Lett.* **2003**, *3*, 1215−1218.
(22) Liang, F.; Sadana, A. K.; Peera, A.; Chattopadhyay, J.; Gu, Z.; Hauge, R. H.; Billups, W. E. *Nano Lett.* **2004**, *4*, 1257−1260.
(23) Chattopadhyay, J.; Sadana, A. K.; Liang, F.; Beach, J. M.; Xiao, Y.; Hauge, R. H.; Billups, W. E. *Org. Lett.* **2005**, *7*, 4067−4069.
(24) Penicaud, A.; Poulin, P.; Derre, A.; Anglaret, E.; Petit, P. *J. Am. Chem. Soc.* **2005**, *127*, 8−9.
(25) Dyke, C. A.; Tour, J. M. *Chem.-Eur. J.* **2004**, *10*, 812−817.
(26) Hirsch, A.; Soi, A.; Karfunkel, H. R. *Angew. Chem.* **1992**, *104*, 808−810 (see also *Angew. Chem., Int. Ed. Engl.* **1992**, *31*, 766−768).
(27) Hirsch, A.; Groesser, T.; Skiebe, A.; Soi, A. *Chem. Ber.* **1993**, *126*, 1061−1067.
(28) Graupner, R.; Abraham, J.; Vencelova, A.; Seyller, T.; Hennrich, F.; Kappes, M. M.; Hirsch, A.; Ley, L. *Phys. Chem. Chem. Phys.* **2003**, *5*, 5472−5476.
(29) Larciprete, R.; Goldoni, A.; Lizzit, S.; Petaccia, L. *Appl. Surf. Sci.* **2005**, *248*, 8−13.
(30) Dresselhaus, M. S.; Eklund, P. C. *Adv. Phys.* **2000**, *49*, 705−814.
(31) Souza Filho, A. G.; Jorio, A.; Samsonidze, G. G.; Dresselhaus, G.; Saito, R.; Dresselhaus, M. S. *Nanotechnology* **2003**, *14*, 1130−1139.
(32) Reich, S.; Thomsen, C.; Maultzsch, J. *Carbon Nanotubes: Basic Concepts and Physical Properties*; Wiley-VCH: Weinheim, 2004.
(33) Dresselhaus, M. S.; Dresselhaus, G.; Saito, R.; Jorio, A. *Phys. Rep.* **2005**, *409*, 47−99.

Scheme 1

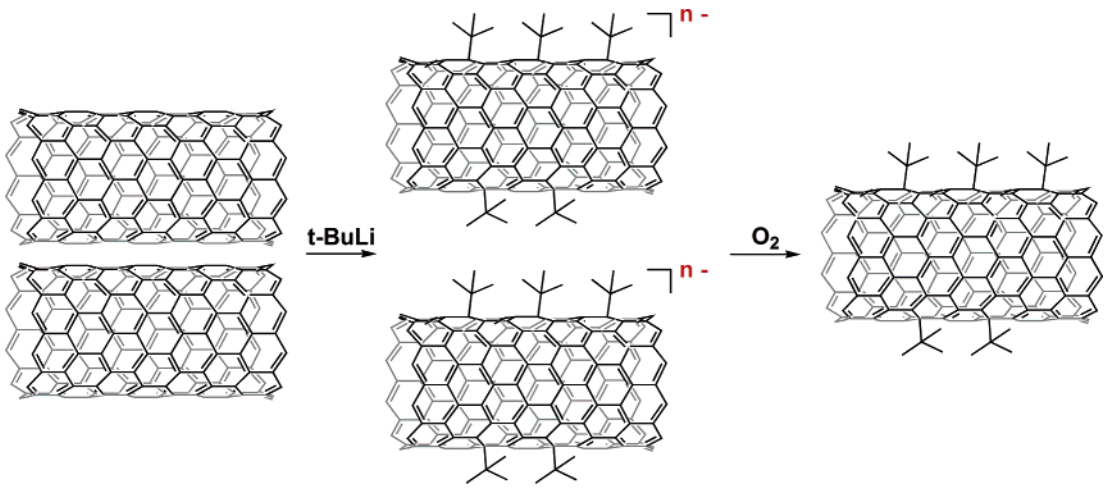

dispersion. During this procedure, the reaction product precipitates. This is a consequence of the charge neutralization, and the SWNTs start to form aggregates again. The formal composition of the reaction products is *t*-Bu$_n$SWNT. In fullerene chemistry, such reoxidation of negatively charged fullerene adducts is known to proceed easily, for example, after exposure to air oxygen or iodine.[9,34] In the case of nanotubes, the oxidation is expected to be even more preferred, because the degree of pyramidalization of the C-atoms of SWNTs is lower than that of fullerenes and carbanions prefer a pyramidalized geometry of the central C-atoms.[10] Workup was achieved by addition of cyclohexane and purging with water and diluted hydrochloric acid in a separation funnel. After filtration through a 0.2 μm PTFE membrane filter, the reaction product was washed with THF, methanol, and ethanol to remove unwanted byproducts. The resulting black solid was dried under vacuum at 50 °C overnight. To increase the degree of functionalization, this reaction sequence was repeated up to three times. The resulting reaction products are denoted as (*t*-Bu$_n$)$_m$SWNT (m = 1−3).

The successful functionalization of the tubes can be deduced by Raman spectroscopy and thermogravimetric analysis. The variation of the amount of *t*-BuLi revealed no change in the degree of functionalization as long as an excess is used. Therefore, we conclude that the degree of functionalization during one reaction sequence is limited because a certain accumulation of negative charge on the SWNTs eventually renders the nanotubes unreactive toward a further nucleophilic attack of *t*-BuLi due to electrostatic repulsion. As a general trend, it can be seen that areas of the D-band and G-band Raman peaks A_D/A_G increase upon going from the starting material to (*t*-Bu$_n$)$_3$-SWNT (Table 1). The increase of the D-band intensity is due to the covalent binding of the addends leading to sp^3-defects in the sidewalls of the tubes. More details of the Raman spectroscopic characterization of *t*-Bu$_n$SWNT will be presented explicitly below.

The weight loss between 85 and 500 °C of the functionalized SWNTs was determined for the calculation of the degree of functionalization expressed by the carbon-to-addend ratio. As can be seen, the degree of functionalization increases with an increasing number of reaction cycles. The highest degree of functionalization, 31, was reached after the third functionalization cycle with the product (*t*-Bu$_n$)$_3$SWNT. This value is comparable to that of the reductive alkylation and arylation protocols developed by Billups and co-workers.[22,23]

Table 1. Raman A_D/A_G Ratios (514.5 nm Excitation) and Weight Loss of Different Compounds from TGA Analysis (80−800 °C in Nitrogen)

compound	A_D/A_G	weight loss (%) observed	carbon/addend ratio
HiPCO SWNTs	0.021		
t-Bu$_n$SWNTs	0.053	13.0	59:1
(*t*-Bu$_n$)$_2$SWNTs	0.053	17.0	36:1
(*t*-Bu$_n$)$_3$SWNTs	0.089	18.6	31:1

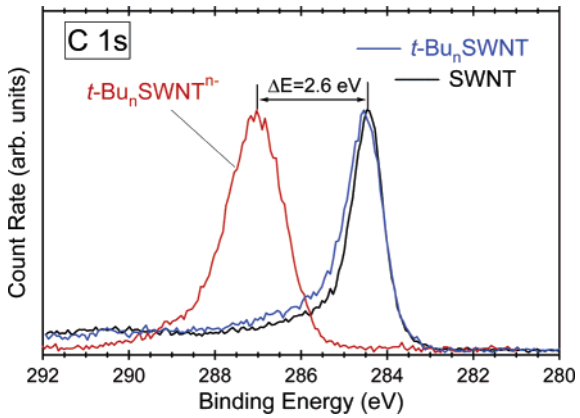

Figure 1. C 1s core level of the starting material (SWNTs), of the charged intermediate *t*-Bu$_n$SWNT^{n-}, and of the reoxidized product *t*-Bu$_n$SWNT.

Photoelectron Spectroscopy. To verify the transfer of negative charge to the SWNTs accompanied by the nucleophilic attack of *t*-BuLi compounds, we decided to carry out a systematic XPS analysis. For this purpose, the reactive intermediate *t*-Bu$_n$SWNT^{n-} was investigated in an in-situ setup. A comparison of the C 1s core level of the *t*-Bu$_n$SWNT^{n-} sample with a spectrum of the starting material is shown in Figure 1. The C 1s core level of the functionalized sample is located at a binding energy that is by 2.6 eV higher than that of the starting material. Several verifications of this experiment always resulted in the same shift of 2.6 ± 0.2 eV.

The C 1s core level shift is explained by the transfer of negative charge to the SWNTs accompanied by the formation of the charged intermediate *t*-Bu$_n$SWNT^{n-}'s (Figure 1). The

(34) Hirsch, A. *Synthesis* **1995**, 895−913.

opposite effect is observed with acid-treated SWNTs, where a positive charge on the SWNTs leads to reduction of the C 1s binding energy.[28] The negative charge on the *t*-Bu$_n$SWNT^{n-}'s is balanced by the positive charge of the Li$^+$-ions. The Coulomb interaction between the charged SWNTs leads to a homogeneous dispersion of the carbon nanotubes in the solvent as the reaction proceeds; it is accompanied by a pronounced exfoliation of the bundles. The charge has to be accommodated by filling previously unoccupied electronic states in the SWNTs. As a result, the Fermi level, E_F, of the *t*-Bu$_n$SWNT^{n-} is higher in energy as compared to the starting material. Because in photoelectron spectroscopy the common reference level of the binding energy is E_F, a change in the position of E_F is reflected in a corresponding binding energy shift of all features in the photoelectron spectra. Similar effects are observed for the stage 1 compound of Li-intercalated graphite, LiC_6, as reported by Wertheim et al.[35] In this study, the C 1s core level of pure graphite was measured at a binding energy of 284.45 eV, identical to our measurements on the SWNTs shown in Figure 1. After the formation of LiC_6, the carbon 1s core level is located at 285.5 eV binding energy. In our measurements, the observed binding energy of the functionalized SWNTs is located at even higher binding energies (287.0 eV). For SWNTs doped by metallic Li, Petaccia et al.[36] and Larciprete et al.[37] recently measured a shift of the C 1s core level of 0.25 eV toward higher binding energy, which is also much lower, as compared to our measurements. The fact that the C 1s core level shifts as a whole, although not all SWNTs are found to be functionalized to the same extent (see below), is caused by the formation of a bucky paper on the sample holder, which leads to the exchange of charge between the individual *t*-Bu$_n$SWNT^{n-} with the development of a common Fermi level for the whole sample. The measured shift of the Fermi level in the solid state therefore corresponds to the average shift over a large number of SWNTs. For the functionalized *t*-Bu$_n$SWNT, no Li was found in the photoelectron spectra, indicating that Li was removed completely. In this sample, the position of the C 1s core level is almost identical to that of the starting material (SWNTs) (Figure 1). This proves that the negative charge on the SWNTs is removed upon oxidation.

The C 1s loss spectra and UPS valence band spectra of *t*-Bu$_n$-SWNT are compared to those of the starting material in Figure 2. The structures on the high binding energy side of the C 1s line (loss spectrum) are caused by electrons that are excited out of the C 1s core level and have undergone characteristic losses due to collective excitations of the electron system. For the SWNTs the loss structure is dominated by the π-plasmon at a loss energy of 5.8 eV[38] (i.e., at 5.8 eV higher binding energy than the C 1s core level, located at 284.45 eV). For the *t*-Bu$_n$-SWNTs, the π-plasmon intensity is almost completely suppressed. Also, the UPS valence band spectra show a significant decrease in intensity between 0 and 4 eV and around 8 eV binding energy. Unfortunately, due to the limited spectral resolution of our spectrometer, we were not able to resolve the

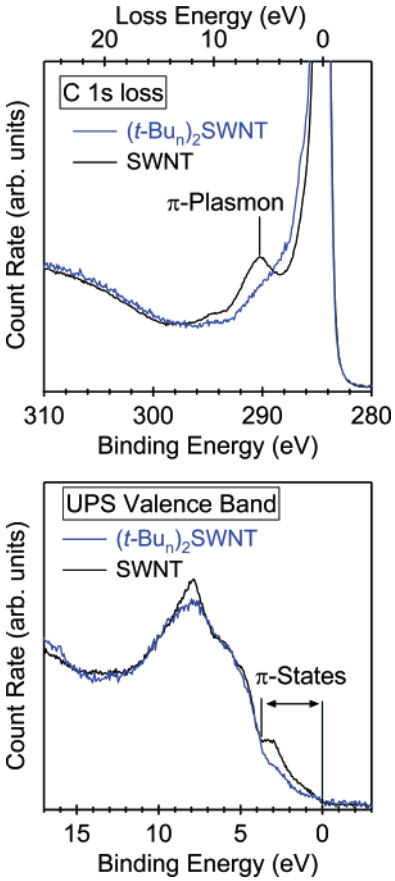

Figure 2. C 1s loss (top) and He II valence band spectra (bottom) of SWNTs as compared to those measured on (*t*-Bu$_n$)$_2$SWNTs.

van-Hove-singularities of the SWNTs;[37,39] therefore, our spectra resemble the ones measured on graphite.[40] The spectral intensity around 3 eV binding energy in graphite is caused by π-states, whereas the states around 8 eV binding energy can be attributed to σ-states.[41] These changes in the spectral intensities show that the rehybridization of the carbon atoms that bear a functional group from an sp^2 to an sp^3 configuration manifests itself in the characteristic changes in the valance band spectra as well as in the reduction of the π-plasmon intensity in the C 1s loss spectra.

Raman Spectroscopy. Figure 3 shows the G-band and the disorder induced D-band of the starting material (SWNT) (bottom line), after the second functionalization (*t*-Bu$_n$)$_2$SWNTs (top curve), and after annealing at 600 °C under nitrogen atmosphere. The G-band of the SWNTs, located at 1590 cm^{-1}, shows the characteristic shoulder toward lower Raman shifts, commonly attributed to the Breit−Wigner−Fano (BWF) resonance of metallic SWNTs.[42] The intensity of this shoulder is considerably reduced after the functionalization procedure, and a significant increase in the D-band intensity is observed as well. Annealing the functionalized tubes (*t*-Bu$_n$)$_2$SWNTs restores the

(35) Wertheim, G. K.; Van Attekum, P. M. T. M.; Basu, S. *Solid State Commun.* **1980**, *33*, 1127−1130.
(36) Petaccia, L.; Goldoni, A.; Lizzit, S.; Larciprete, R. *J. Electron Spectrosc. Relat. Phenom.* **2005**, *144*−*147*, 793−797.
(37) Larciprete, R.; Petaccia, L.; Lizzit, S.; Goldoni, A. *Phys. Rev. B* **2005**, *71*, 115435-1−115435-5.
(38) Pichler, T.; Knupfer, M.; Golden, M. S.; Fink, J.; Rinzler, A.; Smalley, R. E. *Phys. Rev. Lett.* **1998**, *80*, 4729−4732.
(39) Rauf, H.; Pichler, T.; Knupfer, M.; Fink, J.; Kataura, H. *Phys. Rev. Lett.* **2004**, *93*, 096805-1−096805-4.
(40) Chen, P.; Wu, X.; Sun, X.; Lin, J.; Ji, W.; Tan, K. L. *Phys. Rev. Lett.* **1999**, *82*, 2548−2551.
(41) Kihlgren, T.; Balasubramanian, T.; Wallden, L.; Yakimova, R. *Phys. Rev. B* **2002**, *66*, 235422-1−235422-6.
(42) Brown, S. D. M.; Jorio, A.; Corio, P.; Dresselhaus, M. S.; Dresselhaus, G.; Saito, R.; Kneipp, K. *Phys. Rev. B* **2001**, *63*, 155414-1−155414-7.

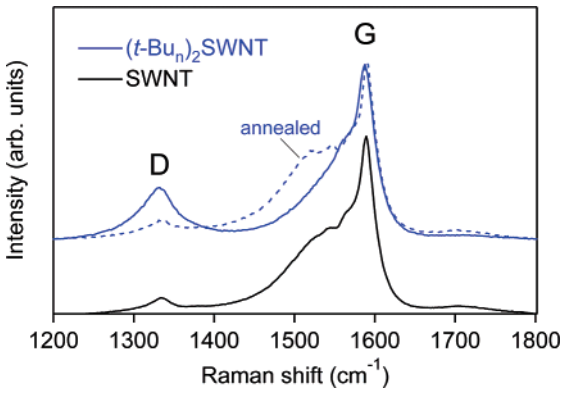

Figure 3. Raman spectra of the G- and D-modes taken at $\lambda_{exc} = 514$ nm. The bottom spectra are taken from the starting material and the top spectra from (t-Bu$_n$)$_2$SWNT. The dashed line is the spectrum taken from the functionalized SWNTs after annealing.

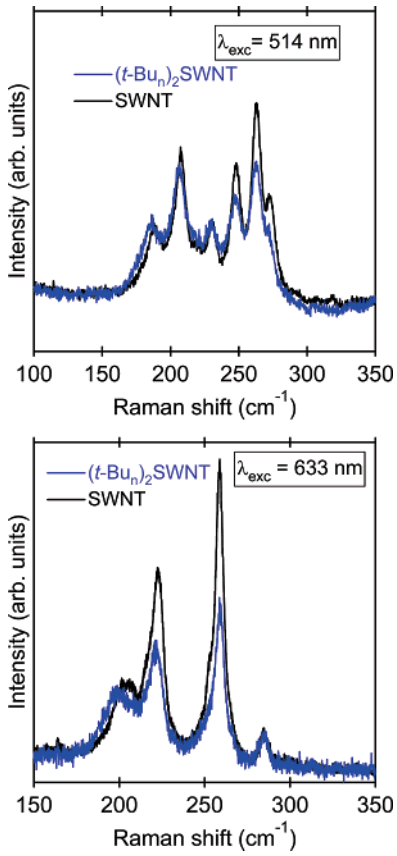

Figure 4. Raman spectra of the radial breathing modes of the starting material as compared to those of (t-Bu$_n$)$_2$SWNT, taken at $\lambda_{exc} = 514$ nm (top) and at $\lambda_{exc} = 633$ nm (bottom). All spectra were normalized to the same integrated G-band intensity from 1450 to 1700 cm^{-1}.

line shape of the G-peak and leads to a reduction of the D-band intensity.

The increase in D-band intensity can be attributed to the disorder induced by the functional groups, while the reduction in the intensity of the BWF-resonance implies a loss of metallic character of the corresponding tubes in the sample. This interpretation is supported by Raman measurements of the RBMs, shown in Figure 4. Here, spectra taken at $\lambda_{exc} = 514$ nm and $\lambda_{exc} = 633$ nm from the starting material are compared to those of (t-Bu$_n$)$_2$SWNT. Note that the presented RBM spectra are normalized to the same integrated intensity of the G-band.

For the spectra measured at $\lambda_{exc} = 514$ nm, a significant decrease in the RBM intensities for the modes above 230 cm^{-1} is observed. For the Raman spectra taken at $\lambda_{exc} = 633$ nm, a reduction in RBM intensities between 220 and 260 cm^{-1} is even more pronounced. Interestingly, the mode at 284 cm^{-1}, which corresponds to the smallest diameter tubes observed for this excitation wavelength, does not show a change in Raman intensity. By comparison of the observed mode frequencies with the so-called "Kataura plot",[43] similar changes in Raman intensities observed at $\lambda_{exc} = 514$ nm by Maeda et al.[44] are interpreted as a separation of metallic and semiconducting SWNTs. A higher reactivity of metallic versus semiconducting SWNTs upon covalent bond formation was also observed in chemical reactions using diazonium salts[45] or dichlorocarbene.[46] In both cases, the higher reactivity is explained by the availability of accessible states close to the Fermi level.[47] The same explanation can be used for our case, where functionalization is accompanied by introduction of negative charge to the SWNTs. As the RBM intensity of the smallest diameter tubes that we observe at $\lambda_{exc} = 633$ nm is not affected by the functionalization, we attribute this mode to small, semiconducting SWNTs. This finding backs the interpretation that indeed the electronic character and not the diameter is decisive for the chemical reactivity of the tubes. However, in interpreting changes in Raman spectra upon functionalization, one has to be careful due to the resonant nature of the Raman scattering process. A decrease in intensity might be caused either by a complete removal of the respective SWNTs or by a change in the electronic structure by the functional groups, which can lead to the situation that the SWNTs fall out of the resonance window. As the line shape of the G-band is restored after annealing, a selective destruction of SWNTs can be ruled out and the latter interpretation seems to be the most likely one.

STM Measurements. STM images of (t-Bu$_n$)$_2$SWNT, taken at 4.7 K, are shown in Figure 5. The image displays a small rope where characteristic protrusions on the sidewalls of all three SWNTs are clearly visible. These protrusions exhibit a threefold symmetry as can be seen in the closer view of the central lower region shown in Figure 6 (top) as well as in the perspective view of a single SWNT (Figure 6, bottom).

It is important to note that the lateral dimensions in the STM images do not represent the true size of a functional group, but rather a convolution of the shape of the STM tip with the molecule located on the SWNT. Therefore, a line profile showing the height variation along the nanotube axis is presented in Figure 5 (bottom). The measured height difference between the tube apex and the functional group is $\Delta z = 1.9$ Å, which has to be compared with the height of the t-butyl-group, which is approximately 2.0 Å. All of these findings unequivocally suggest identifying these characteristic protrusions as the t-butyl groups, introduced by the sidewall functionalization of the SWNTs. In accordance with the results of the Raman spectros-

(43) Kataura, H.; Kumazawa, Y.; Maniwa, Y.; Umezu, I.; Suzuki, S.; Ohtsuka, Y.; Achiba, Y. *Synth. Met.* **1999**, *103*, 2555−2558.
(44) Maeda, Y.; Kimura, S.; Kanda, M.; Hirashima, Y.; Hasegawa, T.; Wakahara, T.; Lian, Y.; Nakahodo, T.; Tsuchiya, T.; Akasaka, T.; Lu, J.; Zhang, X.; Gao, Z.; Yu, Y.; Nagase, S.; Kazaoui, S.; Minami, N.; Shimizu, T.; Tokumoto, H.; Saito, R. *J. Am. Chem. Soc.* **2005**, *127*, 10287−10290.
(45) Strano, M. S.; Dyke, C. A.; Usrey, M. L.; Barone, P. W.; Allen, M. J.; Shan, H.; Kittrell, C.; Hauge, R. H.; Tour, J. M.; Smalley, R. E. *Science* **2003**, *301*, 1519−1522.
(46) Kamaras, K.; Itkis, M. E.; Hu, H.; Zhao, B.; Haddon, R. C. *Science* **2003**, *301*, 1501.
(47) Joselevich, E. *ChemPhysChem* **2004**, *5*, 619−624.

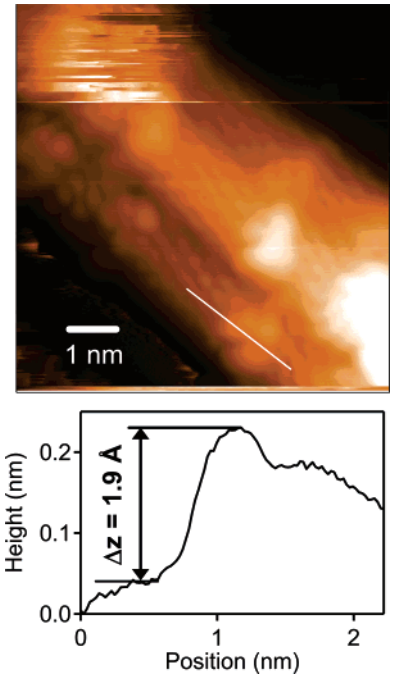

Figure 5. Topographical STM image of (t-Bu$_n$)$_2$SWNTs ($U = -1.0$ V, $I = 0.02$ nA, $T = 4.7$ K). The diagram on the bottom shows the height variation along the line in the STM image.

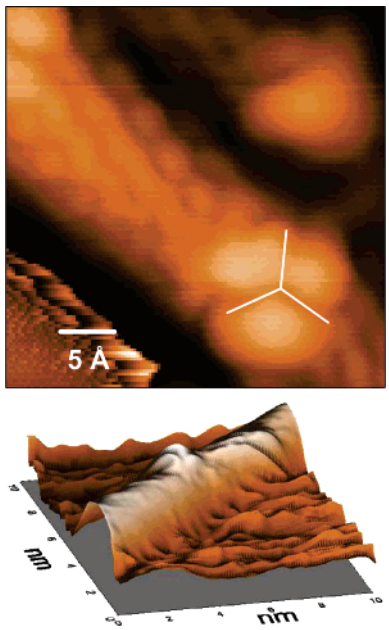

Figure 6. Top: Expanded view of the central lower region of the STM image shown in Figure 5 with a linear background removed. Bottom: Perspective view of an STM image of an individual (t-Bu$_n$)$_2$SWNT ($U = -1.0$ V, $I = 0.3$ nA, $T = 4.7$ K, image size 10 nm × 10 nm). In both images, the three-fold symmetry of the functional group is evident.

copy, not all SWNTs were found to exhibit the same degree of functionalization. Significantly, the rotation of the t-butyl group about the bond between the quaternary C-atoms of the addend and the sidewall of the tube is frozen at 4.7 K. This result is in line with temperature-dependent NMR investigations of t-BuC$_{60}^-$, which showed that the rotation of the t-Bu group is hindered with $\Delta G^{\ddagger} = 9.3$ kcal/mol.[48] In the case of t-Bu$_n$SWNT, the corresponding rotational barrier is expected to be even higher because the C-atoms of HiPco-SWNTs are less pyramidalized than those of C$_{60}$, which makes the rotation of the t-butyl group more difficult. In STM measurements performed at room temperature, it has been observed that the three-fold symmetry of the t-butyl groups attached to the tubes can no longer be resolved and that the addends appear as spherical objects.

Conclusions

We have developed a new reaction sequence for the chemical functionalization of SWNTs. The first step is the treatment of a suspension of the tubes with t-BuLi serving as a strong nucleophile. The nucleophilic addition of the organolithium compound is accompanied by the introduction of one negative charge per addition to the sidewalls of the tubes. As a consequence of this charging process, the reaction intermediates t-Bu$_n$SWNT^{n-} undergo a substantial exfoliation due to electrostatic repulsion. This exfoliation results in the formation of a black homogeneous dispersion of the tubes in benzene, which was used as the solvent. The second step of the reaction sequence is the reoxidation of the anionic intermediates with oxygen leading to the precipitation of the neutral reaction products t-Bu$_n$SWNT. This reaction sequence can be repeated, and the degree of functionalization of the products (t-Bu$_n$)$_m$-SWNT ($m = 1-3$) increases with increasing m. The highest degree of functionalization expressed as the carbon-to-addend ratio of 31 was reached after the third functionalization cycle and is comparable to that of the reductive alkylation and arylation of Billups.[21,22] We also studied this new reaction sequence in detail by photoelectron spectroscopy, Raman spectroscopy, and scanning tunneling microscopy (STM). The C 1s core level spectra reveal that the nucleophilic attack of the t-BuLi leads to negatively charged SWNTs. Upon oxidation, this negative charge is removed. The valence band spectra of the functionalized samples exhibit a significant reduction in the π-derived density of states. In STM, the covalently bonded butyl functionalities manifest themselves as characteristic protrusions showing the three-fold symmetry of the t-butyl addend. The rotation about the CC-bond between the addend and the sidewall of the tubes is frozen at 4.7 K. The G-band in the Raman spectra shows a reduction of the metallicity of the SWNTs, which, together with selective intensity variations in the RBM bands, have been attributed to a preferred functionalization of metallic SWNTs. This selectivity can be explained by the presence of electronic states close to the Fermi level characteristic for metallic but not for semiconducting tubes. These findings suggest that covalent sidewall functionalization of SWNTs, which is accompanied by a charge transfer, opens the possibility to label SWNTs selectively according to their electronic properties. This might ultimately lead to a possible separation process of metallic from semiconducting SWNTs, especially because the parent tubes can be recovered after thermolytical cleavage of the addends. The systematic investigation of the influence of the nucleophilicity of the organometallic reagent on the selectivity of addition will be one important step toward this goal. Work along these lines is currently underway in our laboratories.

Experimental Section

Chemicals and Characterization of the Samples. SWNTs were obtained from Carbon Nanotechnologies Inc. (purified HiPco single-wall carbon nanotubes). Chemicals and solvents were used as received

(48) Fagan, P. J.; Krusic, P. J.; Evans, D. H.; Lerke, S. A.; Johnston, E. *J. Am. Chem. Soc.* **1992**, *114*, 9697−9699.

unless otherwise noted. ^{1}H NMR spectra were recorded on JEOL JMM EX 400 and JEOL GX 400 instruments. XPS spectra were recorded on a Surface Science Instruments, type M-Probe, using a monochromized Al K_α small spot X-ray gun ($\hbar\omega = 1486.6$ eV). Binding energy calibration was carried out by setting the binding energy of the Au 4f 7/2 core level energy at 84.00 eV. For UV-excited photoelectron spectroscopy (UPS) of the valence band, the ultraviolet light of a He gas discharge lamp (He II, $\hbar\omega = 40.8$ eV) was used. As *t*-Bu$_n$SWNT^{n-} is not stable under ambient air, the functionalized SWNTs must be transferred in-situ to the photoemission chamber, that is, without contact to air. This was achieved by dripping the solution containing the functionalized SWNTs from a syringe through a rubber septum into a nitrogen-purged load-lock chamber onto the sample holder. After the solvent was pumped off, a closed "bucky paper" forms on top of the sample holder, which was transferred into the analysis chamber and measured by photoelectron spectroscopy. Raman spectra were recorded either on a Renishaw Ramanscope 2000 equipped with an Ar-laser ($\lambda_{exc} = 514$ nm) or for the detailed measurements of the radial breathing modes (RBMs) on a Jobin Yvon T64000 triple grating spectrometer. Here, an Ar-laser ($\lambda_{exc} = 514$ nm) as well as a He−Ne laser ($\lambda_{exc} = 633$ nm) were used in a confocal microscope setup. The estimated spot size on the sample in this setup is about 2 μm in diameter. The spectra were taken on closed bucky papers of SWNTs and *t*-Bu$_n$SWNT. Special care was taken to keep the laser power on the samples low enough to avoid unwanted thermal effects on the SWNTs. Thermogravimetric analysis (TGA) was accomplished on a Mettler Toledo STDA 811e instrument with the following programmed time-dependent temperature course: 80 °C for 30 min, 80−800 °C with 10 °C/min gradient, and 800 °C for 10 min. STM images were recorded on an Omicron LT-STM, operated at liquid He temperature (4.7 K). The tips for STM measurements were chemically etched Pt−Ir tips. The samples were prepared by spraying a drop of the solution containing the two times functionalized *t*-Bu$_n$SWNTs onto a glass substrate covered by a gold layer, which was previously flame annealed to form Au(111) facets. The density of the SWNTs on the sample was checked by AFM measurements before introduction into the STM chamber.

Geneneral Procedure for the Synthesis of (*t*-Bu$_n$)$_m$SWNT. In a 250 mL nitrogen-purged and heat-dried four-necked round-bottom flask, equipped with two gas inlets and a pressure compensation, 20 mg (1.7 mmol of carbon) of HiPco SWNTs were dispersed in 50 mL of anhydrous benzene under sonication. To this dispersion was added dropwise 4 mL of a 1.7 molar solution of *t*-BuLi (6.8 mmol) in pentane over a period of 10 min. After the completion of the addition, the resulting suspension was stirred for 30 min at room temperature and sonicated for 30 min, resulting in a stable, black, homogeneous dispersion. The reaction mixture was stirred for another hour and subsequently quenched by bubbling oxygen for 30 min through the solution. The resulting heterogeneous dispersion was diluted with 100 mL of cyclohexane, transferred in a separation funnel, and purged with water and diluted hydrochloric acid until the pH value remained neutral. The organic layer with the nanotubes was filtered through a 0.2 μm PTFE membrane filter and washed with THF, methanol, and ethanol. The resulting black solid was dried in a vacuum oven at 50 °C overnight. The whole procedure can be repeated m times with (*t*-Bu$_n$)$_{m-1}$SWNTs ($m = 1-3$) for the synthesis of the higher functionalized (*t*-Bu$_n$)$_m$SWNTs.

Acknowledgment. This work was supported by the "Bayerische Forschungsstiftung" under the auspices of the "Bayerischer Forschungsverbund für Werkstoffe auf der Basis von Kohlenstoff, FORCARBON". Dedicated to Richard Smalley.

Supporting Information Available: XPS C 1s core level spectra of five different samples of the charged intermediate *t*-Bu$_n$SWNT^{n-} as compared to the C 1s spectrum of the starting material (SWNTs). This material is available free of charge via the Internet at http://pubs.acs.org.

JA0607281